METHODS FOR DETERMINING SOIL CONTAMINANT PROFILES FROM PROMPT-NEUTRON GAMMA ACTIVATION DATA

J.K. Shultis, R.E. Faw, and F. Khan, Department of Nuclear Engineering, Kansas State University, Manhattan, KS, 66506

ABSTRACT This paper summarizes three mathematical models used to describe how contaminant concentration profiles in soil may be inferred from the intensities of neutron-induced capture-gamma photon intensities measured at the soil surface. In particular, the linear regularization, linear regularization with an iterative positivity constraint, and the Backus-Gilbert methods are applied to the soil contamination problem. Examples of each of the three methods are presented for idealized test contaminant profiles.

KEYWORDS: PGNAA, soil, inversion methods, contamination profiles

INTRODUCTION

In the prompt-gamma neutron-activation analysis (PGNAA) method, soil is illuminated by a beam or source of fast neutrons and the subsequent capture gamma photons produced when these neutrons are absorbed by elemental contaminants in the soil are measured at, or slightly above, the surface. For a given contaminant, capture photons with (usually) many distinct characteristic energies are emitted. The uncollided capture photons that are emitted by each element and that reach the surface are measured, and from these measured intensities the concentration of a particular contaminant at different depths can be estimated.

To estimate soil contamination profiles from the intensities of uncollided gamma photons measured above the soil surface, it is first necessary to develop a mathematical model that relates contaminant concentration profiles to the detector measurements. In the next section two idealized soil irradiation geometries are considered, and the fundamental relation between the detector measurement and the soil contaminant profile is derived. In later sections three modern approaches for inverting the PGNAA model to obtain the contaminant profile from measurements of uncollided capture gamma intensities at the soil surface are summarized and example results are given.

PGNAA SOIL CONTAMINATION MODEL

In this study we assume that the soil surface is a flat horizontal plane and that the soil composition and contaminant concentrations vary only with depth x into the soil, i.e., no lateral variations are considered. The two PGNAA models developed in this section differ in how the soil is irradiated by fast neutrons. In the first model, normally incident fast neutrons uniformly illuminate the soil surface to produce a neutron fluence in the soil that varies spatially only with depth. In the second model, the soil is irradiated by a point source of fast neutrons

that produces a fluence with dependence on both depth and lateral distance.

Capture-gamma photon source strengths

Central to the development of any PGNAA mathematical model that relates a contaminant profile to detector measurements is the determination of the number of capture gamma photons emitted at every position in the soil exposed to the neutrons.

Consider first the case in which the soil is illuminated by a monoenergetic perpendicular beam of fast neutrons. The strength of the neutron irradiation is denoted by J_o which is the number of neutrons crossing each unit area of the soil surface. This flow of neutrons results in an energy-dependent fluence $J_o\ddot{\Phi}(x,E)$ at depth x. If the atomic concentration of contaminant j is denoted by $u_j(x)$ (u for *unknown*), the number of neutrons absorbed by this contaminant, per unit volume, at depth x is

$$A_j(x) = J_o u_j(x)\int_0^{E_o} dE\,\hat{\Phi}(x,E)\sigma_c^j(E), \qquad (1)$$

where $\sigma_c^j(E)$ is the microscopic absorption cross section of element j for neutrons with energy E, and E_o is the energy of the incident neutrons.

As verified by Faw, *et al.* [1], the shape of the epithermal energy spectrum is almost independent of depth. Further, most neutrons are absorbed only after they have been thermalized. Thus the total neutron absorption can be described in terms of the thermal fluence by defining an effective capture cross section $\bar{\sigma}_c^j$ as

$$\bar{\sigma}_c^j \equiv \frac{1}{\hat{\Phi}_{th}(x)}\int_0^{E_o} dE\,\hat{\Phi}(x,E)\sigma_c^j(E), \qquad (2)$$

where $\ddot{\Phi}_{th}(x)$ is the thermal fluence at depth x, per unit incident neutron flow, and is obtained by integrating $\ddot{\Phi}(x,E)$ over all thermal energies. For most contaminants the effective capture cross section is remarkably close to the actual thermal absorption cross section—a good indication that most neutron absorption occurs only after thermalization [1].

With this effective capture cross section, the total neutron absorption rate A_j can then be computed knowing only the thermal fluence, namely $A_j(x) = J_o\bar{\sigma}_c^j u_j(x)\Phi_{th}(x)$. For each thermal neutron absorbed by contaminant element j, f_i^j capture photons of energy E_i are emitted. Capture photon yields for nonthermal neutrons are usually not known, and in this study are assumed to equal those for thermal neutron absorption. Moreover, since most neutrons are absorbed only after thermalization, the use of thermal capture yields for all neutron energies is a reasonable approximation. Finally, the number $S_i(x)$ of capture photons with energy E_i that are emitted per unit soil volume at depth x as a result of neutron capture in contaminant j is calculated from

$$S_i^j(x) = J_o f_i^j \bar{\sigma}_c^j u_j(x)\hat{\Phi}_{th}(x). \qquad (3)$$

Before the source strength of capture gamma photons can be determined by Equation 3, the thermal fluence profile $\ddot{\Phi}_{th}(x)$ must first be determined. In another phase of this project, empirical expressions based on detailed neutron transport calculations are obtained for $\ddot{\Phi}_{th}(x)$ for five representative soils [1, 2]. Example fluence profiles for uniform and perpendicular

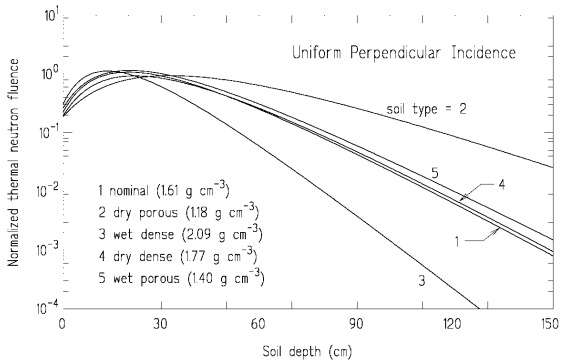

FIGURE 1. THERMAL FLUENCE PROFILES IN THE FIVE REPRESENTATIVE SOILS USED IN THIS STUDY. THE SOIL SURFACE IS UNIFORMLY AND PERPENDICULARLY IRRADIATED BY 14-MeV NEUTRONS WITH A UNIT INWARD FLOW AT THE SURFACE.

illumination of the soil surface by 14-MeV neutrons are shown in Figure 1.

For the case that the soil is irradiated by a point source a distance h_s above the soil surface, the neutron fluence $\ddot{\Phi}(r,x,E)$ in the soil is a function of both the depth x and the radial distance r from the vertical axis through the source. In general, such a neutron source is collimated so that only those neutrons emitted a downward cone of directions, whose axis is perpendicular to the soil surface, reach the soil. Thus, if the source emits S_o monoenergetic neutrons isotropically with energy E_o, the total number flowing into the soil is $J_o = S_o(1 - \cos\theta_s)/2$ where θ_s is the conical half-angle of the source collimation. Again the thermal neutron absorption can be described in terms of the same effective capture cross section used for parallel beam illumination and the thermal neutron fluence profile $\ddot{\Phi}_{th}(r,x)$. Thus the capture photon source strength per unit volume of soil $S_i^j(r,x)$ is given by Equation 3, with $\ddot{\Phi}_{th}(r)$ replaced by $\ddot{\Phi}_{th}(r,x)$. Again empirical expressions based on detailed neutron transport calculations have been obtained for $\ddot{\Phi}_{th}(r,x)$ for five representative soils [1, 2].

PGNAA model for uniform illumination

In this irradiation geometry, the soil is uniformly and perpendicularly illuminated by a parallel fast neutron beam. The capture-gamma photons are measured by a point isotropic detector which is at height h_d above the surface and which is conically collimated downward with a conical half-angle of θ_d.

Consider a horizontal annular volume of radius r, radial thickness dr, and vertical thickness dx that is at depth x and coaxial with the vertical axis through the detector. All points in this differential annular volume of $dV = 2\pi r\, dr\, dx$ are at a distance $y = \sqrt{r^2 + (x + h_d)^2}$ from the detector, so that the uncollided fluence at the detector of ith type photons emitted by element j is

$$dR_i^j = \frac{S_i^j(x)\,dV}{4\pi y^2}\exp\left[-\mu(E_i)x/\cos\theta\right], \tag{4}$$

where $\cos\theta = (x + h_d)/y$, and $\mu(E_i)$ is the total attenuation coefficient (less the coherent scattering component) in soil for a photon of energy E_i. The volumetric source strength S_i^j of ith energy photons from element j in the annular volume is given by Equation 3. Integration of Equation 4 over all r and x within the detector's cone of collimation then gives

$$R_i^j = J_o f_i^j \bar{\sigma}_c^j \int_0^\infty dx\, u_j(x)\hat{\Phi}_{th}(x) \int_0^{(x+h_d)\tan\theta_d} dr \frac{r}{2\left[r^2 + (x+h_d)^2\right]}\exp\left[-\mu(E_i)x/\cos\theta\right]. \tag{5}$$

The integral over r can be performed analytically and expressed in terms of the exponential integral function $E_1(x)$. The result is

$$R_i^j = J_o f_i^j \bar{\sigma}_c^j \int_0^\infty dx u_j(x) \hat{\Phi}_{th}(x) \left[E_1\left(\mu_i x\right) - E_1\left(\mu_i x \sec\theta_d\right) \right] / 2, \tag{6}$$

where $\mu_i \equiv \mu(E_i)$. Finally this fluence of uncollided photons of energy E_i produces a detector measurement or count of $c_i^j = \eta_i R_i^j$ where η_i is the detector efficiency for recording a count in the photopeak per incident photon of energy E_i. Although the efficiency of a real detector may also depend on the incident direction of the photon and the count rate (resulting in *dead time* losses), these effects are not considered in this study. Multiplication of Equation 5 by the detector efficiency yields the following Fredholm integral equation of the first kind for the concentration profile for the jth contaminant, $u_j(x)$,

$$c_i^j = \int_0^\infty dx u_j(x) r_i^j(x), \quad i = 1,\ldots,N_j, \tag{7}$$

where N_j is the number of distinct capture-photon energies measured for contaminant j, and $r_i^j(x)$ is the *response kernel* given by

$$r_i^j(x) = \eta_i J_o f_i^j \bar{\sigma}_c^j \hat{\Phi}_{th}(x) \left[E_1\left(\mu_i x\right) - E_1\left(\mu_i x \sec\theta_d\right) \right] / 2. \tag{8}$$

Equation 7 is the fundamental relation between the contaminant concentration profile and the measured intensities of capture gamma photons. From this equation, we must estimate the concentration profile $u(x)$ from the measured values of c_i.

PGNAA model for a point source

When the soil is irradiated by a point, downward conically-collimated, neutron source of strength S_o, $\ddot{\Phi}_{th}$ is a function of r as well as x. Thus, Equation 5 must be modified to

$$R_i^j = J_o f_i^j \bar{\sigma}_c^j \int_0^\infty dx u_j(x) \int_0^{(x+h_d)\tan\theta_d} dr \frac{r \hat{\Phi}_{th}(r,x)}{2\left[r^2 + \left(x+h_d\right)^2\right]} \exp\left[-\mu_i x / \cos\theta\right], \tag{9}$$

where J_o is the number of source neutrons entering the soil. Multiplication of this result by the detector efficiency η_i results in the same Fredholm integral equation as was obtained for the parallel beam case, namely Equation 7, except that the response kernel $r_i^j(x)$ is now given by

$$r_i^j(x) = J_o \eta_i f_i^j \bar{\sigma}_c^j \int_0^{(x+h_d)\tan\theta_d} dr \frac{r \hat{\Phi}_{th}(r,x)}{2\left[r^2 + \left(x+h_d\right)^2\right]} \exp\left[-\mu_i x / \cos\theta\right], \tag{10}$$

The integral in Equation 10 can no longer be performed analytically unless some analytical approximation is made for $\ddot{\Phi}_{th}(r,x)$, such as a piecewise constant representation. Discussion of the numerical evaluation of this normalized kernel for the five representative soils considered in this study is presented by Shue and Faw [2].

INVERSION BY LINEAR REGULARIZATION

In the previous section, the detector response c_i to the ith capture-gamma photon emitted by a particular elemental contaminant is given by Equation 7, namely

$$c_i = \int_0^\infty dx u(x) r_i(x), \quad i = 1,\ldots,N. \tag{11}$$

(For simplicity, the elemental index j is suppressed from now on since each elemental contaminant profile can be determined separately and the responses from each different contaminant are independent.) The solution of Equation 11 for the contaminant concentration profile is an inversion problem encountered in many diverse fields. For example this same inversion problem (but with different kernels) is encountered in oil-well logging, neutron scattering, geophysical data analysis, atmospheric remote sensing, astrophysics, medical tomography, and many other data analysis applications.

The principal difficulty with solving this equation for the unknown profile $u(x)$ in the PGNAA soil contamination problem is that the number N of different photopeak counts c_i is generally much less than the number of depths at which one would like to determine $u(x)$. Although most heavy atom contaminants typically emit dozens or even hundreds of capture-gamma photons with different energies, most are emitted with such low probabilities or yields that accurate measurement of their intensities are usually not possible. Only very few (typically 2 to 8) capture gamma photons have yields above 10% and, consequently, in practical applications of the PGNAA method, N is almost always a small integer.

In this section, the linear regularization method is used to obtain an inversion of Equation 11. This particular approach goes by many names (e.g., Tikhonov-Miller regularization [3-6], Phillips-Twomey method [7, 8], constrained linear inversion method [9], and the method of regularization [10]). As with any method that has evolved from many different disciplines, the notation and ideas in the many seminal works are often quite different. In our discussion of this and the other inversion methods discussed in this report, we adhere closely to the nomenclature and excellent presentation by Press, *et al.* [11].

Discretization of the model

The first step is to approximate Equation 11 by a set of linear equations for the concentration $u_j \equiv u(x_j)$ at M specified depths x_j by using some appropriate numerical quadrature scheme to approximate the integral. The resulting linear equations can be written as

$$c_i = \sum_{j=1}^{M} R_{ij} u_j, \quad i = 1, \ldots, N, \tag{12}$$

or in matrix notation $\mathbf{c} = \mathbf{R} \bullet \mathbf{u}$.

This set represents N equations in the M unknowns $\{u_j\}$. Here the N x M matrix $\mathbf{R}$ depends on the numerical quadrature approximation selected. For example, suppose the contaminant concentration is negligible beyond a certain depth $x_M \equiv x_{max}$ so that Equation 11 can be approximated by

$$c_i \cong \int_0^{x_{\max}} dx\, r_i(x) u(x) = \sum_{j=1}^{M-2}{}' \int_{x_j}^{x_j+2} dx\, r_i(x) u(x) \tag{13}$$

where the prime on the summation indicates that the summation is over only odd values of j. For the approximation developed here, M is assumed odd. Now approximate $u(x)$ in each pair of adjacent subintervals by a quadratic function. For equally spaced nodes with $\Delta x = x_j - x_{j-1}$, $u(x)$ in interval (x_{j-1}, x_{j+1}) is approximated by

$$u(x) = \frac{(x - x_j)(x - x_{j+1})}{2\Delta x^2} u_{j-1} + \frac{(x - x_{j-1})(x - x_{j+1})}{\Delta x^2} u_j + \frac{(x - x_{j-1})(x - x_j)}{2\Delta x^2} u_{j+1}. \quad (14)$$

Substitution of this result into Equation 13 gives Equations 12 where the R_{ij} are given by

$$R_{ij} = \frac{1}{2\Delta x^2} \begin{cases} \int_{x_1}^{x_3} dx (x - x_2)(x - x_3) r_i(x), & j = 1 \\ \int_{x_{j-1}}^{x_{j+1}} dx (x - x_{j-1})(x - x_{j+1}) r_i(x) \\ + \int_{x_j}^{x_{j+2}} dx (x - x_{j+1})(x - x_{j+2}) r_i(x), & j \text{ even} \\ \int_{x_{j-2}}^{x_j} dx (x - x_{j-2})(x - x_{j-1}) r_i(x), & j \text{ odd}, j \neq 1, M \\ \int_{x_{M-2}}^{x_M} dx (x - x_{M-2})(x - x_{M-1}) r_i(x), & j = M \end{cases} \quad (15)$$

Difficulty in inverting the discretized model

The inversion of Equation 12 is an ill-posed problem since the number of unknowns M (the u_j) is generally greater than the number N of data (the c_i). This means there are an infinite number of solutions because the solution space (of dimension M) has an (M - N) dimensional degeneracy, i.e., any (M - N) components of **u** can be specified arbitrarily and still have Equation 12 satisfied.

One might be tempted to solve Equation 12 by minimizing the difference between some model $\hat{\mathbf{u}}(x)$ and the measured data. This difference between a model and measured data is often quantified by the χ^2 statistic, namely

$$\chi^2 = \sum_{i=1}^{N} \sum_{j=1}^{M} \left[c_i - \sum_{k=1}^{M} R_{ik} \hat{u}_k \right] S_{ij}^{-1} \left[c_j - \sum_{k=1}^{M} R_{jk} \hat{u}_k \right] \quad (16)$$

$$\approx \sum_{i=1}^{N} \frac{1}{\sigma_i^2} \left[c_i - \sum_{k=1}^{M} R_{ik} \hat{u}_k \right]^2 = |\mathbf{A} \bullet \hat{\mathbf{u}} - \mathbf{b}|^2. \quad (17)$$

Here S_{ij} = Covar[n_i, n_j] are the elements of the covariance matrix with n_i being the uncertainty or random noise associated with the measured c_i. The approximate equality in the above result holds if we can neglect the off-diagonal covariance terms, with σ_i^2 = Covar[n_i, n_i]. The matrix **A** has elements $A_{ij} = R_{ij}/\sigma_i$ and the vector **b** has elements $b_i = c_i/\sigma_i$. For the counting data of uncollided capture gamma photons used in the soil contamination problem, the estimate of σ_i is $\sqrt{c_i}$ provided c_i is sufficiently large (typically greater than a few hundred counts).

The minimum value of χ^2 is zero and is obtained with a $\hat{\mathbf{u}}$ which is a solution of

$$\mathbf{A} \bullet \hat{\mathbf{u}} = \mathbf{b}. \quad (18)$$

Such a set of linear equations with a non-square matrix **A** (or a singular square matrix **A**) can be "solved" by the singular value decomposition (SVD) method [11]. This method produces the *least-squares solution* for an overdetermined system (**A** has more rows than columns, i.e., $N > M$). The real power of the SVD method, however, is to treat singular or underdetermined systems for which there are an infinity of solutions to Equation 18. Among the infinity of degenerate solutions (most of which have very large values of $\hat{u}_i$) the SVD method will select the one that has the smallest norm $||\hat{\mathbf{u}}||$. This solution, called the *principal solution*, will produce a value of χ^2 that is zero (or nearly so). Such a result is quite unrealistic. Theoretically, the true profile $u(x)$ should yield a value of $\chi^2 \approx N$ since the χ^2 distribution approaches, as N becomes large, a normal distribution with mean N and standard deviation $\sqrt{2N}$. Clearly, a modified approach must be taken for our "underdetermined" problem.

Regularization of the underdetermined system

Consider an "unknown" vector **u** that we want to find as a solution to some minimization problem involving two positive functionals $\mathcal{A}[\mathbf{u}] > 0$ and $\mathcal{B}[\mathbf{u}] > 0$. We may wish to find **u** as the vector that minimizes $\mathcal{A}[\mathbf{u}]$ subject to the constraint $\mathcal{B}[\mathbf{u}] = b$, i.e., with the Lagrange multiplier λ_b,

$$\frac{\delta}{\delta \mathbf{u}}\left\{\mathcal{A}[\mathbf{u}] + \lambda_b\left(\mathcal{B}[\mathbf{u}] - b\right)\right\} = \frac{\delta}{\delta \mathbf{u}}\left\{\mathcal{A}[\mathbf{u}] + \lambda_b \mathcal{B}[\mathbf{u}]\right\} = 0. \tag{19}$$

Alternatively, we may want to find **u** as the vector (generally a different vector) that minimizes $\mathcal{B}[\mathbf{u}]$ subject to the constraint $\mathcal{A}[\mathbf{u}] = a$, i.e., with the Lagrange multiplier λ_a,

$$\frac{\delta}{\delta \mathbf{u}}\left\{\mathcal{B}[\mathbf{u}] + \lambda_a\left(\mathcal{A}[\mathbf{u}] - a\right)\right\} = \frac{\delta}{\delta \mathbf{u}}\left\{\mathcal{B}[\mathbf{u}] + \lambda_a \mathcal{A}[\mathbf{u}]\right\} = 0. \tag{20}$$

If we identify $\lambda \equiv \lambda_a$ as $1/\lambda_b$ we see that the above two results are identical minimization problems. Both cases yield the same one-parameter family of solutions, say $\mathbf{u}(\lambda)$. As λ varies from 0 to ∞, the solution $\mathbf{u}(\lambda)$ varies along the *trade-off curve* between minimizing $\mathcal{A}$ (subject to constraint $\mathcal{B} = b$) and minimizing $\mathcal{B}$ (subject to constraint $\mathcal{A} = a$).

Now for the important theorem. Suppose that the functional $\mathcal{A}[\mathbf{u}]$ has the following form:

$$\mathcal{A}[\mathbf{u}] = |\mathbf{A} \bullet \mathbf{u} - \mathbf{b}|^2 \tag{21}$$

for a matrix **A** that is degenerate, i.e., has fewer rows than columns. Then the minimization of $\mathcal{A}[\mathbf{u}]$ will not give a unique solution for **u**. However, if we add any non-degenerate quadratic form $\mathcal{B}[\mathbf{u}]$, for example $\mathbf{u}\bullet\mathbf{H}\bullet\mathbf{u}$, then the minimization of $\mathcal{A}[\mathbf{u}] + \lambda\mathcal{B}[\mathbf{u}]$ *will* produce a unique solution **u** [11]! The addition of the term $\lambda\mathcal{B}[\mathbf{u}]$ is said to "regularize" the minimization problem, i.e., to produce a unique solution.

Thus in the inverse problem, to obtain a unique solution for **u**, one solves the following minimization problem

$$\text{minimize:} \qquad \mathcal{A}[\mathbf{u}] + \lambda\mathcal{B}[\mathbf{u}]. \tag{22}$$

This is the central principle of inversion theory. As λ varies from 0 to ∞, the unique solution **u** varies from minimizing $\mathcal{A}[\mathbf{u}]$ to minimizing $\mathcal{B}[\mathbf{u}]$. To obtain the "best" solution (corresponding to a particular value of λ) one must choose a particular criterion. For example, one might pick λ so that $\chi^2 = N$ agrees with the expected value of χ^2. Alternatively, one might pick λ purely subjectively so as to produce, for example, a "smooth" solution or a solution sensitive to abrupt changes in the profile $u(x)$. Finally, for simulated count data obtained by accurate numerical integration of Equation 11, the most accurate inversion will be obtained with λ made as small as possible, but still large enough to avoid numerical instabilities in the minimization algorithm.

The linear regularization method

The many apparently different approaches used for inversion problems all involve minimizing the functional of Equation 22 with the choice for $\mathcal{A}[\mathbf{u}]$ and $\mathcal{B}[\mathbf{u}]$ dependent on the problem and the inversion philosophy. In the linear regularization approach, the functional $\mathcal{A}[\mathbf{u}]$ of Equation 22 is taken as the χ^2 of Equation 17, i.e., $\mathcal{A}[\mathbf{u}] = |\mathbf{A}\bullet\mathbf{u} - \mathbf{b}|^2$, and the functional $\mathcal{B}[\mathbf{u}]$ is

chosen as some measure of the smoothness of $u(x)$, which is derived from first or higher derivatives of $u(x)$. In particular, the linear regularization method requires that $\mathcal{S}[\mathbf{u}] = \hat{\mathbf{u}}\bullet\mathbf{H}\bullet\hat{\mathbf{u}}$ where $\mathbf{H}$ is some appropriate smoothing matrix. The inversion solution is thus determined by the following minimization problem:

$$\text{minimize:} \qquad \mathcal{A}[\mathbf{u}] + \lambda\mathcal{S}[\mathbf{u}] = |\mathbf{A}\bullet\hat{\mathbf{u}} - \mathbf{b}|^{2} + \lambda\hat{\mathbf{u}}\bullet\mathbf{H}\bullet\hat{\mathbf{u}}. \qquad (23)$$

The matrix $\mathbf{H}$ is obtained by making some *a priori* assumption about the nature of the profile $u(x)$. Several examples are given in the next section.

To obtain the minimum of the functional of Equation 23 and find $\hat{\mathbf{u}}$, we write Equation 23 in its component form as

$$\mathcal{F}[\mathbf{u}] \equiv \mathcal{A}[\mathbf{u}] + \lambda\mathcal{S}[\mathbf{u}] = \sum_{i=1}^{N}\left[\sum_{j=1}^{M} A_{ij}\hat{u}_j - b_i\right]^2 + \lambda\sum_{i=1}^{M}\hat{u}_i\sum_{j=1}^{M} H_{ij}\hat{u}_j. \qquad (24)$$

The values of $\hat{u}_j$ that minimize this functional are the solutions of the *M normal equations* obtain by setting the derivative of $\mathcal{F}[\mathbf{u}]$ with respect to $\hat{u}_j$ to zero. Differentiation of Equation 24 with respect to $\hat{u}_j$, setting the result to zero, and use of the symmetry property of $\mathbf{H}$ gives

$$\sum_{j=1}^{M}\left\{\left(\sum_{i=1}^{N} A_{ik}A_{ij}\right) + \lambda H_{jk}\right\}\hat{u}_j = \sum_{i=1}^{M} A_{ik}b_i, \qquad k = 1,\ldots,M, \qquad (25)$$

or in matrix form,

$$\left(\mathbf{A}^T \bullet \mathbf{A} + \lambda\mathbf{H}\right)\bullet\hat{\mathbf{u}} = \mathbf{A}^T \bullet \mathbf{b}. \qquad (26)$$

This equation can be solved for $\hat{\mathbf{u}}$ by standard means, such as the *LU* decomposition or SVD methods [11].

Smoothing matrices

The construction of the M x M matrix $\mathbf{H}$ depends on the *a priori* smoothness criterion chosen. For example, if we believe that $u(x)$ is approximately linear, then a reasonable functional to minimize so as to enforce this belief is (assuming equi-spaced values of x_j)

$$\mathcal{S}[\mathbf{u}] \propto \int_0^\infty \left[\hat{u}''(x)\right]^2 dx \propto \sum_{j=1}^{M-2}\left[-\hat{u}_j + 2\hat{u}_{j+1} - \hat{u}_{j+2}\right]^2. \qquad (27)$$

Note that this functional is nonnegative and vanishes only when $\hat{u}(x)$ is a linear function. The constant of proportionality can be absorbed into the parameter λ so that the discretized form of $\mathcal{S}[\mathbf{u}]$ can be written as

$$\mathcal{S}[\mathbf{u}] = |\mathbf{B}\bullet\hat{\mathbf{u}}|^2 = \hat{\mathbf{u}}\bullet\left(\mathbf{B}^T\bullet\mathbf{B}\right)\bullet\hat{\mathbf{u}} = \hat{\mathbf{u}}\bullet\mathbf{H}\bullet\hat{\mathbf{u}}, \qquad (28)$$

where $\mathbf{B}$ is the (M - *2*) x M first-order, forward finite-difference matrix

$$\mathbf{B} = \begin{pmatrix} -1 & 2 & -1 & 0 & 0 & 0 & 0 & \ldots & 0 \\ 0 & -1 & 2 & -1 & 0 & 0 & 0 & \ldots & 0 \\ \vdots & & & & \ddots & & & & \vdots \\ 0 & \ldots & 0 & 0 & 0 & -1 & 2 & -1 & 0 \\ 0 & \ldots & 0 & 0 & 0 & 0 & -1 & 2 & -1 \end{pmatrix}. \qquad (29)$$

If we believe a quadratic function is a good approximation for $u(x)$ then we should minimize (again use forward finite differences)

$$\mathcal{S}[\mathbf{u}] \propto \int_0^\infty \left[\hat{u}'''(x)\right]^2 dx \propto \sum_{j=1}^{M-3}\left[-\hat{u}_j + 3\hat{u}_{j+1} - 3\hat{u}_{j+2} + \hat{u}_{j+3}\right]^2 \qquad (30)$$

so that

$$\mathbf{B} = \begin{pmatrix} -1 & 3 & -3 & 1 & 0 & 0 & 0 & \ldots & 0 \\ 0 & -1 & 3 & -3 & 1 & 0 & 0 & \ldots & 0 \\ \vdots & & & & \ddots & & & & \vdots \\ 0 & \ldots & 0 & 0 & -1 & 3 & -3 & 1 & 0 \\ 0 & \ldots & 0 & 0 & 0 & -1 & 3 & -3 & 1 \end{pmatrix}. \qquad (31)$$

Similarly, for cubic smoothing, we attempt to minimize

$$\begin{aligned}\mathcal{E}[\mathbf{u}] &\propto \int_0^\infty \left[\hat{u}''''(x)\right]^2 dx \\ &\propto \sum_{j=1}^{M-4}\left[-\hat{u}_j + 4\hat{u}_{j+1} - 6\hat{u}_{j+2} + 4\hat{u}_{j+3} - \hat{u}_{j+4}\right]^2\end{aligned} \tag{32}$$

so that

$$\mathbf{B} = \begin{pmatrix} -1 & 4 & -6 & 4 & -1 & 0 & 0 & \dots & 0 \\ 0 & -1 & 4 & -6 & 4 & -1 & 0 & \dots & 0 \\ \vdots & & & & \ddots & & & & \vdots \\ 0 & \dots & 0 & -1 & 4 & -6 & 4 & -1 & 0 \\ 0 & \dots & 0 & 0 & -1 & 4 & -6 & 4 & -1 \end{pmatrix}. \tag{33}$$

In fact the choice of **B** or **H** can be obtained from any finite difference representation of the function $u(x)$, such as a discretized differential equation.

Example results

To determine the capabilities of the linear regularization method for application to the soil contamination problem, several idealized contaminant profiles were used. With these test profiles for $u(x)$, simulated values of c_i were evaluated from Equation 11 using an adaptive Gaussian numerical integration algorithm which is capable of achieving high accuracy. The thermal fluence profile used in the kernel $r_i(x)$ of Equation 8 was one of those shown in Figure 1 for the five standard soils used in this study. For the examples presented below, chromium is the assumed contaminant and, usually, only the five capture gamma photons with yields greater than 10% are used in the simulation. An example set of simulated c_i data generated in this manner is given in Table 1. These values of c_i, which are used in several of the examples below, are for an idealized detector that produces no statistical uncertainty in the measured c_i. Thus for all the examples in this section, the standard deviations σ_i of the c_i are taken as unity. In later studies the effect of statistical uncertainties in the simulated data is to be investigated.

TABLE 1. CALCULATED C_i VALUES FOR CHROMIUM CONTAMINATED SOIL DISTRIBUTED WITH THE BILINEAR PROFILE SHOWN IN FIGURE 2. PROBLEM PARAMETERS: FLUENCE PROFILE 4 (DRY DENSE SOIL); $J_o = 1$; $\eta_i = 1$; $\theta_d = \pi/2$.

Energy (MeV)	Yield per capture	μ_i (cm^{-1})	c_i
0.7492	.1104	0.130030	9.31146
0.8351	.2686	0.123690	22.5795
7.9393	.1275	0.043362	9.12322
8.8841	.2697	0.042026	19.1419
9.7203	.1097	0.041009	7.73532

With such simulated data for c_i, test contaminant profiles were inverted and compared to the actual profiles shown by the heavy dashed lines in the figures following. Additional examples are presented by Shultis, *et al.* [12].

The inverted contaminant profile depends strongly on the parameter λ that balances the trade-off between smoothness and accuracy of the profile to the measured c_i. The smaller λ the better is the fit to the data, i.e., the smaller $\chi^2 \equiv \mathcal{A}[\mathbf{u}] \equiv |\mathbf{A}\bullet\mathbf{u} - \mathbf{b}|^2$ becomes. By contrast, as λ becomes large, the inverted profile becomes smoother and the fit becomes less accurate, i.e., $\hat{\mathbf{u}}\bullet\mathbf{H}\bullet\hat{\mathbf{u}}$ becomes smaller while χ^2 becomes larger. This behavior is illustrated in Figure 2 which shows profiles for extreme values of λ. In these examples, for $\lambda \geq 10$ the inverted profile assumes a strict linear shape as

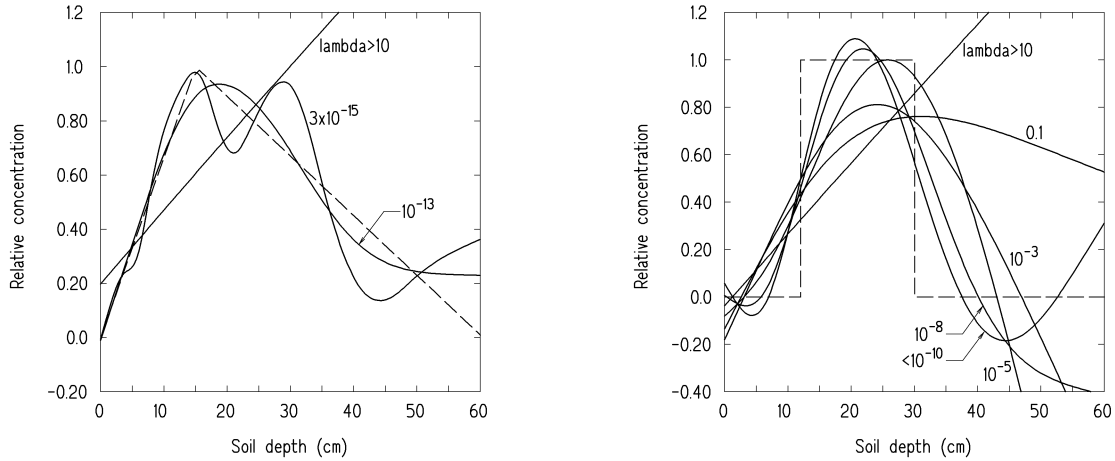

FIGURE 2. INVERTED PROFILES FOR A CHROMIUM CONTAMINANT USING LINEAR REGULARIZATION WITH LINEAR SMOOTHING FOR SEVERAL VALUES OF λ. THE EXACT PROFILE IS SHOWN BY THE HEAVY DASHED LINE. PROBLEM PARAMETERS: SOIL TYPE 4; $\theta_d = \pi/2$; MINIMUM PHOTON YIELD 10% (5 PHOTONS); NUMBER OF SUBLAYERS 51; PIECEWISE QUADRATIC DISCRETIZATION; $J_o = 1$; $\eta_i = 1$.

prescribed by the linear smoothing constraint used. At the other extreme when $\lambda = 10^{-13}$ the inverted profile agrees very closely with the actual profile. However, if λ is made even smaller, the effect of the smoothing regularization term is lost because of the finite precision of the computer, and numerical instabilities begin to develop as shown in the profile on the lefthand side of Figure 2 obtained with $\lambda = 3 \times 10^{-15}$.

Since the simulated c_i values used in these examples are exact, i.e., have no associated statistical uncertainties, the optimal (most accurate) inverted profile is obtained with the smallest value of λ that can be used before numerical instabilities appear. These best-fit profiles, i.e., those with the smallest χ^2, represent the maximum capability of the inversion method since any real data for the c_i will have uncertainties and thus contain less information for the inversion process. In Figure 3 optimally resolved inverted profiles for the bilinear and step profiles are shown for the three smoothing regularization methods considered in the study. As can be seen, the inverted profiles are quite reasonable, especially for the bilinear case in the lefthand side of Figure 3. All three regularization methods give nearly the same results, differing primarily at large and shallow soil depths where spurious negative and positive variations are characteristically produced.

The righthand figure in Figure 3 also demonstrates the effect of using different numbers of capture gamma photons. Generally, as more photons, i.e., more c_i, are used the better are the inverted results. However the increased accuracy in going from 5 chromium photons (minimum capture photon yield 10%) to 10 photons (minimum yield 6%) is surprisingly slight. All three smoothing methods produce nearly identical results for the Gaussian peak. Only for the spurious oscillations at deep depths where $u(x)$ is negligibly small, do differences become apparent for the three smoothing

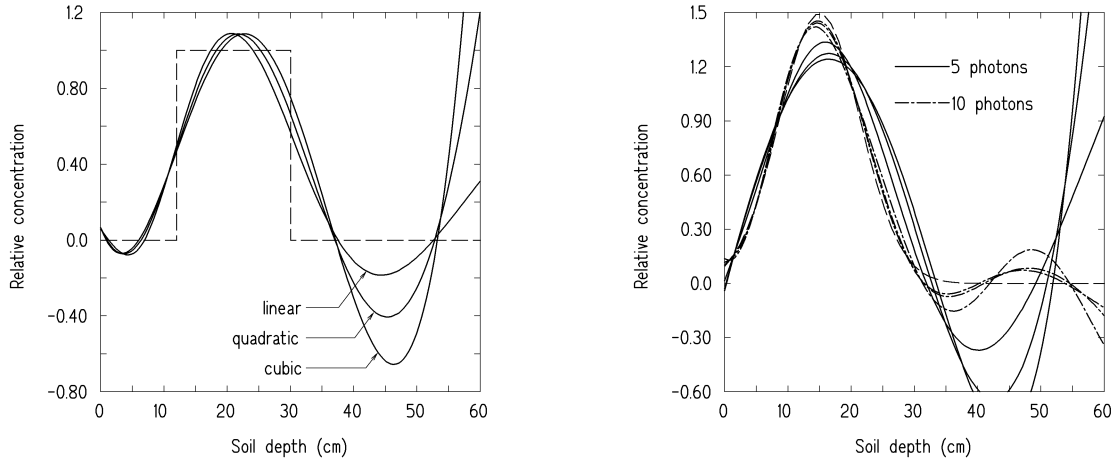

FIGURE 3. OPTIMAL INVERSION OF TWO TEST PROFILES (HEAVY DASHED LINES) FOR A CHROMIUM CONTAMINANT USING LINEAR, QUADRATIC, AND CUBIC REGULARIZATIONS. THESE MAXIMALLY RESOLVED PROFILES ARE OBTAINED WITH $\lambda \cong 10^{-9}$. PROBLEM PARAMETERS: SOIL TYPE 4; $\theta_d = \pi/2$; MINIMUM PHOTON YIELD 10% (5 PHOTONS) OR 6% (10 PHOTONS—RIGHTHAND FIGURE); NUMBER OF SUBLAYERS 51; PIECEWISE QUADRATIC DISCRETIZATION; $J_o = 1$; $\eta_i = 1$.

schemes and for the number of photons used.

As seen in these examples, the linear regularization method is capable of extracting quite reasonable profiles given only a small number of c_i values (here 5). However, the inverted profiles for all three regularization methods typically exhibit large negative and even positive concentrations at large (optical) depths in the soil where $u(x)$ is usually extremely small. Also when $u(x)$ is small near the surface, the inverted profiles often yield negative concentration estimates. These spurious false values are a characteristic artifact of the inversion process since linear regularization imposes no positivity constraint on the $\hat{u}(x)$.

One simplistic approach is simply to ignore such negative concentration estimates and set the offending value to zero. Similarly large positive values at great depth may be false and should likewise be ignored, particularly if preceded by a region of negative estimates. However, such an ad hoc procedure is not very satisfying. In the next section a more rigorous approach is suggested which incorporates a positivity constraint directly into the inversion process.

CONSTRAINED LINEAR REGULARIZATION METHOD

Often we want the solution $\hat{u}(x)$ to be constrained in some manner in addition to minimizing $\mathcal{A}[\mathbf{u}] + \lambda\mathcal{B}[\mathbf{u}]$. For example, we may want $\hat{u}(x) \geq 0$ or $u_L(x) \leq \hat{u}(x) \leq u_U(x)$ for specified functions u_L and u_U. The method of *projections onto convex sets* (POCS) is an easy way to impose such deterministic constraints if an iterative solution of the functional minimization problem is used. In this section we outline how a functional minimization problem can be performed iteratively and then how deterministic constraints can be superimposed on such an iterative solution.

Many iterative schemes can be used to find the $\hat{u}(x)$ which minimizes the functional $\mathcal{A}[\mathbf{u}]+\lambda\mathcal{B}[\mathbf{u}]$, ranging from the conjugate gradient method [11] to specialized algorithms such as those proposed by Skilling [13-15]. An unsophisticated approach is to use the method of steepest descent, whereby we approach the minimum of $\mathcal{A}[\mathbf{u}]+\lambda\mathcal{B}[\mathbf{u}]$ by proceeding from some arbitrary starting point in $\hat{\mathbf{u}}$ space by taking small steps always in the direction opposite the gradient of $\mathcal{A}[\mathbf{u}]+\lambda\mathcal{B}[\mathbf{u}]$. That is, as we step through $\hat{\mathbf{u}}$ space, we always head "downhill." Mathematically, the iteration search is

$$\hat{\mathbf{u}}^{(k+1)} = \hat{\mathbf{u}}^{(k)} - \varepsilon\nabla(\mathcal{A}[\mathbf{u}] + \lambda\mathcal{B}[\mathbf{u}]) \tag{34}$$

where ε is a parameter that determines how far to move downhill in each step. For the linear regularization method, based on minimizing the functional $\mathcal{A}[\mathbf{u}] + \lambda\mathcal{B}[\mathbf{u}] = |\mathbf{A}\bullet\mathbf{u} - \mathbf{b}|^2 + \lambda\hat{\mathbf{u}}\bullet\mathbf{H}\bullet\hat{\mathbf{u}}$ (see Equation 23), the minimization iteration scheme becomes

$$\begin{aligned}\hat{\mathbf{u}}^{k+1} &= \hat{\mathbf{u}}^{(k)} - \varepsilon\nabla\left(|\mathbf{A}\bullet\hat{\mathbf{u}} - \mathbf{b}|^2 + \lambda\hat{\mathbf{u}}\bullet\mathbf{H}\bullet\hat{\mathbf{u}}\right)\\ &= \hat{\mathbf{u}}^{(k)} - 2\varepsilon\left[\left(\mathbf{A}^T\bullet\mathbf{A} + \lambda\mathbf{H}\right)\bullet\hat{\mathbf{u}} - \mathbf{A}^T\bullet\mathbf{b}\right]\\ &= \left[1 - \varepsilon\left(\mathbf{A}^T\bullet\mathbf{A} + \lambda\mathbf{H}\right)\right]\bullet\hat{\mathbf{u}}^{(k)} + \varepsilon\mathbf{A}^T\bullet\mathbf{b},\end{aligned} \tag{35}$$

where, to guarantee convergence [11],

$$0 < \varepsilon < \frac{1}{\text{max eigenvalue}\left(\mathbf{A}^T\bullet\mathbf{A} + \lambda\mathbf{H}\right)}. \tag{36}$$

Now return to the problem of imposing deterministic constraints on our iterative solution. First two definitions. A set of vectors $\{\hat{\mathbf{u}}\}$ defines a *convex set* if, for any two elements $\hat{\mathbf{u}}_a$ and $\hat{\mathbf{u}}_b$, the vector $(1-\eta)\hat{\mathbf{u}}_a + \eta\hat{\mathbf{u}}_b$, $0 \le \eta \le 1$, is also in the set. For example, constraints such as all components of $\hat{\mathbf{u}}$ must be (1) positive, or (2) zero outside some upper and lower bounds define convex sets.

Of special utility for convex sets are *nonexpansive projection operators* $\mathcal{P}_i$ defined such that $\mathcal{P}_i$ first leaves unchanged any $\hat{\mathbf{u}}$ already in a convex set C_i, and second $\mathcal{P}_i$ maps any vector outside C_i to the closest vector in C_i. Recipes like "set all negative components of $\hat{\mathbf{u}}$ to zero" or "set all components less than some lower bound to that bound and all components greater than an upper bound to that bound" are simple word descriptions of nonexpansive projective operators.

The importance of these two concepts is the following extraordinary theorem quoted by Press [11]. If C is the intersection of m convex sets $C_1, C_2,\ldots,C_m$, then the iteration

$$\hat{\mathbf{u}}^{(k+1)} = \left(\mathcal{P}_1\mathcal{P}_2\ldots\mathcal{P}_m\right)\hat{\mathbf{u}}^k \tag{37}$$

converges to a point in C from all starting points as $k \to \infty$. If C is empty, then there is no convergence. Thus, if we pick $\mathcal{P}_1$ as the projection operator that sets to zero all negative components of $\hat{\mathbf{u}}$, the following modification of Equation 35

$$\hat{\mathbf{u}}^{k+1} = \mathcal{P}_1\left\{\left[1 - \varepsilon\left(\mathbf{A}^T\bullet\mathbf{A} + \lambda\mathbf{H}\right)\right]\bullet\hat{\mathbf{u}}^{(k)} + \varepsilon\mathbf{A}^T\bullet\mathbf{b}\right\} \tag{38}$$

converges to the vector with nonnegative components, which minimizes $\mathcal{A}[\mathbf{u}] + \lambda\mathcal{B}[\mathbf{u}]$ for the linear regularization method.

Examples for the constrained linear regularization method

In Figure 4 the iterative solution based on Equation 38 for a chromium contaminant step profile is show along with the profile obtained with the linear regression method. Results for two different starting profiles are

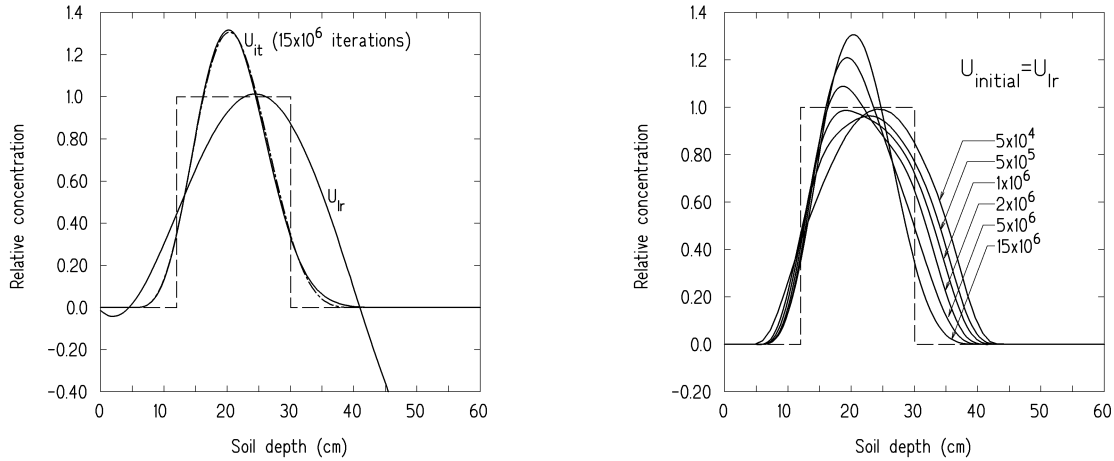

FIGURE 4. INVERSION OF THE STEP PROFILE FOR A CHROMIUM CONTAMINANT USING CONSTRAINED ITERATIVE LINEAR REGULARIZATION FOR $\lambda = 0.001$ USING A VARYING NUMBER OF ITERATIONS (RIGHTHAND) AND DIFFERENT STARTING PROFILES (LEFTHAND FIGURE). THE EXACT PROFILE IS SHOWN BY THE HEAVY DASHED LINE. IN THE RIGHTHAND FIGURE THE ITERATIONS BEGIN WITH $u_{initial}(x) = u_{lr}(x)$. PROBLEM PARAMETERS: SOIL TYPE 4; $\theta_d = \pi/2$; MINIMUM PHOTON YIELD 10% (5 PHOTONS); NUMBER OF SUBLAYERS 51; PIECEWISE QUADRATIC DISCRETIZATION; CUBIC SMOOTHING; $J_o = 1$; $\eta_i = 1$.

shown in the lefthand figure. The solid line is for an iterative solution with the linear regularization solution as the starting profile (labeled as U_{lr}), while the dash-dotted line is for an iterative solution obtained with a null initial profile. That the two iteratively calculated profiles are almost identical indicates that the iterations have converged and are independent of the starting profile. From this figure it is seen that the iterative constrained method produces a much better estimation of the contaminant profile than does the unconstrained linear regularization method.

In the righthand example of Figure 4, the iterative solutions for different numbers of iterations are shown. To obtain a converged solution for this example takes a very large number of iterations. This is characteristic of the constrained iteration method [11]. The achievement of a completely converged iterative solution is computationally expensive; nevertheless, the iterative result obtained before convergence is still a better estimate of the contaminant profile than is the linear regression solution which often exhibits unrealistic negative values of concentration at small and deep distances into the soil. Moreover, even before convergence, the constrained iterative method produces results that are more accurate than the linear regularization solution. In practical applications full convergence is thus often not required.

Constrained iterative results for two other test profiles are shown in Figure 5. It is seen from these figures that the constrained iteration method produces inverted profiles that agree much more closely with the actual profiles than does the linear regularization method. One important feature of the constrained iterative solution is that the

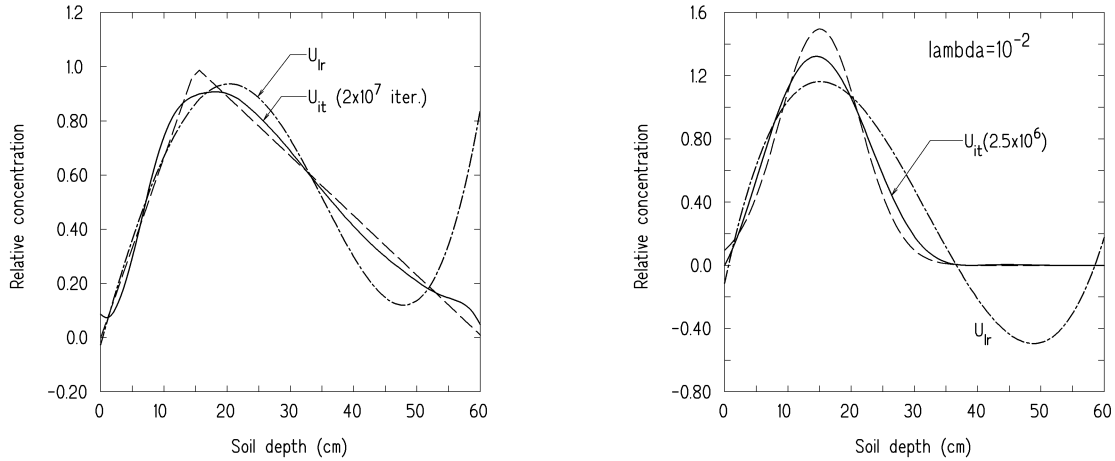

FIGURE 5. INVERSION OF THE BILINEAR PROFILE (LEFTHAND FIGURE) AND GAUSSIAN PROFILE (RIGHTHAND FIGURE) FOR A CHROMIUM CONTAMINANT USING CONSTRAINED ITERATIVE LINEAR REGULARIZATION METHOD. THE EXACT PROFILES ARE SHOWN BY THE HEAVY DASHED LINES. PROBLEM PARAMETERS: SOIL TYPE 4; $\theta_d = \pi/2$; MINIMUM PHOTON YIELD 10% (5 PHOTONS); NUMBER OF SUBLAYERS 51; CUBIC SMOOTHING, PIECEWISE QUADRATIC DISCRETIZATION; $J_o = 1$; $\eta_i = 1$.

inverted profile is less sensitive to the assumed value of λ than is the linear regularization solution. This effect is seen in Figure 4 where the iterative solutions for $\lambda = 10^{-4}$ and $\lambda = 10^{-6}$ are seen to be very similar compared to the linear regularization solutions. Since λ, which specifies the balance between smoothness and accuracy is difficult to determine *a priori*, the constrained iterative method is very attractive, not only because it eliminates unrealistic negative concentrations, but also because it is relatively insensitive to λ.

THE BACKUS-GILBERT METHOD

The Backus-Gilbert method [11, 16-19] is different from other regularization methods in its special selection of the functionals $\mathcal{A}$ and $\mathcal{B}$. For $\mathcal{B}$ the method maximizes the stability of the solution $\hat{u}(x)$ rather than its smoothness. In particular, the Backus-Gilbert method uses the variance of the estimated profile $\hat{u}(x)$, i.e.,

$$\mathcal{B} \equiv Var[\hat{u}(x)] \tag{39}$$

as a measure of how much the solution $\hat{u}(x)$ varies as the data vary within their measurement errors. It must be emphasized that this variance is not the expected deviation of the $\hat{u}(x)$ from the true $u(x)$ but rather it is the variance of the expected experiment-to-experiment scatter among estimates $\hat{u}(x)$ if the whole experiment were to be repeated many times.

For the functional $\mathcal{A}$, the Backus-Gilbert method tries to make $\hat{u}(x)$ as close to $u(x)$ as possible. Since the method is linear, $\hat{u}(x)$ is related to $u(x)$ as follows

$$\hat{u}(x) = \int_0^\infty dx' \, \hat{\delta}(x', x) u(x'), \tag{40}$$

where $\delta(x',x)$ is the so-called *resolution function* or *averaging kernel*. The Backus-Gilbert method seeks to minimize the spread of $\hat{\delta}$, i.e., maximize the resolving power, so that abrupt discontinuities in $u(x)$ can be detected. Consequently, the functional $\mathcal{A}$ is chosen to be some positive measure of the spread.

Starting with Equation 11 for c_i, and imposing linearity from the start, we seek a set of *inverse response kernels* $q_i(x)$ such that

$$\hat{u}(x) = \sum_i q_i(x) c_i \,, \tag{41}$$

where $\hat{u}(x)$ is the desired estimator of $u(x)$. Toward this end, we define the integral of the response kernel for each data point,

$$R_i \equiv \int_0^\infty dx\, r_i(x). \tag{42}$$

Substitution of Equation 41 into Equation 11, and comparison of the result with Equation 40, shows that the averaging kernel is given by

$$\hat{\delta}(x',x) = \sum_i q_i(x) r_i(x'). \tag{43}$$

We also require that this kernel should have unit normalization for every x, so that

$$\begin{aligned} 1 = \int_0^\infty dx' \hat{\delta}(x',x) &= \sum_i q_i(x) \int_0^\infty dx' r_i(x') \\ &= \sum_i q_i(x) R_i \\ &= \mathbf{q}(x) \bullet \mathbf{R}, \end{aligned} \tag{44}$$

where $\mathbf{q}(x)$ and $\mathbf{R}$ are each vectors of length N, the number of measurements. The functional $\mathcal{B}$ can now be expressed in terms of $\mathbf{q}(x)$. Standard propagation of errors and application of Equation 39 gives

$$\begin{aligned} \mathcal{B} = Var[\hat{u}(x)] &= \sum_i \sum_j q_i(x) S_{ij} q_j(x) \\ &= \mathbf{q}(x) \bullet \mathbf{S} \bullet \mathbf{q}(x), \end{aligned} \tag{45}$$

where $\mathbf{S}$ is the covariance matrix. If the off-diagonal covariances are neglected as is done in this paper, then this matrix is simply $S_{ij} = \delta_{ij}\sigma_i^2$.

We now need to define the measure of the spread of $\delta(x',x)$ at each x. While many choices are possible, the Backus-Gilbert method chooses the second moment of the square of the averaging kernel. This choice becomes the functional $\mathcal{A}$, namely,

$$\begin{aligned} \mathcal{A} &= \int_0^\infty dx' (x'-x)^2 \left[\hat{\delta}(x',x)\right]^2 \\ &= \sum_i \sum_j q_i(x) W_{ij}(x) q_j(x) \\ &= \mathbf{q}(x) \bullet \mathbf{W}(x) \bullet \mathbf{q}(x), \end{aligned} \tag{46}$$

where $\mathbf{W}(x)$ is the N x N *spread matrix* whose elements are defined as

$$W_{ij} \equiv \int_0^\infty dx' (x'-x)^2 r_i(x') r_j(x'). \tag{47}$$

The function $q_i(x)$ is now selected as the function that minimizes the functional $\mathcal{A} + \lambda\mathcal{B}$. Thus we must solve the following minimization problem

$$\text{minimize:} \qquad \mathcal{A} + \lambda\mathcal{B} = \mathbf{q}(x) \bullet \left[\mathbf{W}(x) + \lambda\mathbf{S}\right] \bullet \mathbf{q}(x) \tag{48}$$

subject to the constraint of Equation 44 that requires $\mathbf{q}(x)\bullet\mathbf{R}$ to equal unity. The solution of Equation 48 is [12]

$$\mathbf{q}(x) = \frac{\left[\mathbf{W}(x) + \lambda\mathbf{S}\right]^{-1} \bullet \mathbf{R}}{\mathbf{R} \bullet \left[\mathbf{W}(x) + \lambda\mathbf{S}\right]^{-1} \bullet \mathbf{R}}. \tag{49}$$

For any particular set of data $\mathbf{c}$, whose elements are the measurements c_i, the solution $\hat{u}(x)$ is formally given by

$$\hat{u}(x) = \frac{\mathbf{c} \bullet \left[\mathbf{W}(x) + \lambda \mathbf{S}\right]^{-1} \bullet \mathbf{R}}{\mathbf{R} \bullet \left[\mathbf{W}(x) + \lambda \mathbf{S}\right]^{-1} \bullet \mathbf{R}} . \tag{50}$$

Equations 49 and 50 are of a completely different nature from the linearly regularized equations. The vectors and matrices in Equations 49 and 50 are all of size N, the number of measurements. There is no discretization of x, so M does not come into play at all. In this method one solves a different N x N set of linear equations for each desired value of x. By contrast, in the linear regularization method one solves an M x M linear set only once. Thus, the computational effort of repeatedly solving linear systems makes the Backus-Gilbert method unsuitable for any but one-dimensional problems such as the present PGNAA soil contamination problem.

Choosing the numerical value for λ in this method depends on the desired solution of a particular problem. If one needs a more stable solution, then a higher value of λ should be chosen, and, if one requires a more resolved solution, a lower value of λ should be chosen. As the value of λ is changed, one sees very explicitly the trade-off between the conflicting demands of resolution and stability in the solution. In the above analysis, there is no reason that λ must be a constant; one can thus pick λ to be a function of x, $\lambda = \lambda(x)$.

Example calculations

In order to assess the capabilities of the Backus-Gilbert method for application to the soil contamination problem, several test profiles were used [12]. For brevity, only two examples are presented here. For these examples, chromium is the soil contaminant, and the five gamma photons with yields greater than 10% were used in the simulation. The values of c_i were calculated very accurately from Equation 11 by using an adaptive Gaussian numerical integration algorithm so that the standard deviation of c_i is very small and hence is taken as unity for all the test problems. The effect of statistical uncertainty in the simulated data will be investigated in later studies.

The symmetry of the **W** matrix ensures that the inverted profiles are nonnegative. This guaranteed positivity of the inverted profile is an obvious advantage of the Backus-Gilbert method over the linear regularization method. Less obvious is the ability of this method to yield the maximum resolution for sudden changes in the concentration profile. Comparison of the Backus-Gilbert inverted profile in Figure 6 to that of the linear regularization inverted profiles in Figure 3 shows that the sharp discontinuities of the test step concentration profile are better deduced by the Backus-Gilbert method.

From the example results in Figure 6 it is seen that the inverted profile again depends strongly on the parameter λ, which balances the trade-off between stability and resolution of the inverted profile. The smaller λ the better the resolution of the inverted profile. On the other hand, a larger value of λ corresponds to a numerically more stable inverted profile. This stability is achieved at the expense of resolution.

CONCLUSIONS

From the results of this study, it has been shown that the three regularization methods presented here are capable of estimating concentration profiles from a surprisingly few measured intensities of capture gamma photons. Although the linear regularization

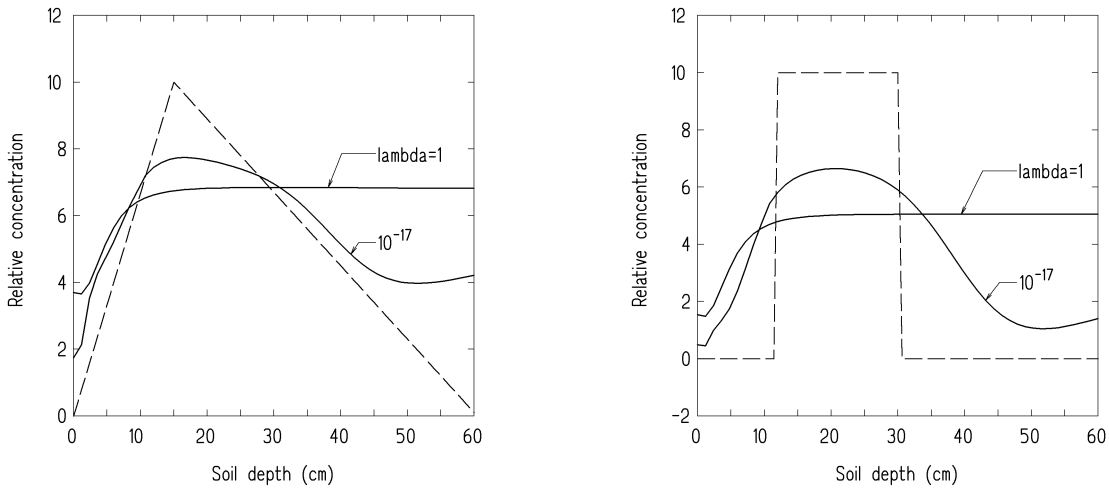

FIGURE 6. THE INVERTED BILINEAR AND STEP PROFILES USING THE BACKUS-GILBERT METHOD FOR SEVERAL VALUES OF λ. THE EXACT PROFILES ARE SHOWN BY THE DASHED LINES. PROBLEM PARAMETERS; SOIL TYPE 4; $\theta_d = \pi/2$; MINIMUM YIELD = 10% (5 PHOTONS); NUMBER OF SUBLAYERS 51; $J_o = 1$; $\eta_i = 1$.

method is the most computationally efficient method, it suffers from the tendency to produce spurious negative or positive values at large soil depths. While the linear regularization method with iterative positivity constraints avoids this difficulty, it is computationally very expensive and useful only when detailed predictions are needed. The Backus-Gilbert technique was found to produce not only nonnegative profiles but profiles while yielding good resolution for abrupt changes in the contaminant concentrations. These conclusions are based on analyses of simulated data without statistical measurement error. Future work will assess the importance of such errors on the ability of the different inversion methods to predict contaminant profiles.

REFERENCES

1. R.E. Faw, J.K. Shultis, B.C. Letellier, S.L. Shue, and F.A. Khan, First Quarter Progress Report: PGNAA Applications in Characterization of Contaminated Soils, HSRC-94-02-06, Kansas State University, Manhattan, Kansas, 1995.

2. S.L. Shue and R.E. Faw, Penetration of 14 MeV Neutron into Representative Soils, HSRC-94-02-09, Kansas State University, Manhattan, Kansas, 1996.

3. A.N. Tikhonov, The approximate solution of Fredholm integral equations of the first kind, Zh. Vych. Mat., 4 (1964) 564-571.

4. A.N. Tikhonov and V.Y. Arsenin, Solutions of Ill-Posed Problems, John Wiley and Sons, New York, 1977.

5. K. Miller, SIAM Journal on Mathematical Analysis, 1 (1970) 52-74.

6. J. Biemond, R.L. Lagendijk, and R.M. Mersereau, Proceedings of the IEEE, 78 (1990) 856-883.

7. D.L. Phillips, Journal of the Association for Computing Machinery, 9 (1962) 84-97.

8. S. Twomey, Journal of the Association for Computing Machinery, 10 (1963) 97-101.

9. S. Twomey, Introduction to the Mathematics of Inversion in Remote Sensing and Indirect Measurements, Elsevier, Amsterdam, 1977.

10. I.J. Craig and J.C. Brown, Inverse Problems in Astronomy, Adam Hilger, Bristol, UK, 1986.

11. W.H. Press, S.A. Teukolsky, W.T. Vetterling, and B.P. Flannery, Numerical Recipes in FORTRAN, chapter 18, Cambridge University Press, 2nd ed., 1992.

12. J.K. Shultis, R.E. Faw, and F.A. Khan, Mathematical Models and Analysis for PGNAA of Soil Contamination, HSRC-94-02-10, Kansas State University, Manhattan, Kansas, 1996.

13. J. Skilling and S.F. Gull, Algorithms and applications, Maximum-Entropy and Bayesian Methods in Inverse Problems, University of Wyoming, 1985, pp. 83-132.

14. J. Skilling, Maximum Entropy and Bayesian Methods in Applied Statistics, Cambridge, Cambridge University Press, 1986.

15. J. Skilling (Ed.), Maximum Entropy and Bayesian Methods, Cambridge, England, August 1-5, 1988.

16. G.E. Backus and J.F. Gilbert, Numerical applications of a formalism for geophysical inverse problems, Geophys. J. R. Astr. Soc., 13 (1967) 247-276.

17. G.E. Backus and F. Gilbert, Resolving power of gross Earth data, Geophys. J. R. Astr. Soc., 16 (1968) 169-205.

18. R.L. Parker, Understanding inverse theory, Annual Review of Earth and Planetary Sciences, 5 (1977) 35-64.

19. T.J. Loredo and R.I. Epstein, Analyzing gamma-ray burst spectral data, Astrophysical Journal, 336 (1989) 896-919.